53rd International Annual Conference of the Fraunhofer ICT
Convention Center, Karlsruhe, Germany (June 25-June 28, 2024)

UCM/MMP cookoff models for explosives containing HMX

Michael L. Hobbs, Michael J. Kaneshige, William W. Erikson
Sandia National Laboratories,[*] Albuquerque, NM 87185, USA

Abstract

We have had success in modeling cookoff of explosives by using a Universal Cookoff Model (UCM) that was first presented at the 50th ICT meeting. This model was improved by coupling to a MicroMechanics Pressurization (MMP) model. One drawback of the combined UCM/MMP model is insufficient parameterization for our explosives of interest. Here, we use historic data from the Sandia Instrumented Thermal Ignition (SITI) experiment to create UCM/MMP models of octahydro-1,3,5,7-tetranitro-1,3,5,7-tetrazocine (HMX) containing explosives such as EDC-37 (HMX, nitrocellulose, K10 binder: 91/1/8 wt.%), HMX (pure), LX-07 (HMX, Viton-A: 90/10 wt.%), LX-10 (HMX, Viton-A 95:5 wt.%), LX-14 (HMX, Estane®: 95.5/4.5 wt.%), PBX 9501 (HMX/Estane®/nitroplasticizer: 95/2.5/2.5 wt.%), and PBXN-9: (HMX/polybutadiene binder or PB/dioctyl adipate or DOA: 92/2/6 wt.%). The models are validated with SITI data from Sandia National Laboratories (SNL) and one-dimensional time-to-explosion (ODTX) data from Lawrence Livermore National Laboratory (LLNL).

Introduction

Exposing confined explosives to high temperatures is extremely dangerous. Heat and confinement cause exothermic decomposition rates to accelerate until heat generation surpasses dissipation leading to thermal ignition. In the current work we present seven cookoff models that can be used for safety analysis of explosives containing HMX.

In 2019 [1], we presented a Universal Cookoff Model (UCM) that determines thermal ignition time using 1) a moisture desorption reaction, 2) a condensed-phase reaction, 3) a gas-phase pressure-dependent reaction, and 4) a binder reaction. The explosives were assumed to be permeable with pressure being spatially uniform. Pressure increases were caused by both decomposition and temperature changes. The permeable assumption is not ideal for high-density-explosives where decompositions gases can be trapped in defects dispersed throughout the explosive causing spatially varying pressure. In 2021 [2], we relaxed the "permeable" assumption by using a MicroMechanics Pressurization (MMP) model where local pressure is determined by solving the displacement equations for a symmetric linear elastic material surrounding a pressurizing hollow sphere. The combined model is referred to as a UCM/MMP cookoff model.

In 2024 [3], we have simplified the UCM model by eliminating the moisture desorption reaction and combining the other three reactions. The reasons for simplification are 1) most explosives of interest have little or no moisture that appreciably affect ignition time and 2) separating the two-explosive reaction from the binder reaction implies reaction products do not interact. This simplified UCM model was tested using seven diverse explosives that contain hexahydro-1,3,5-trinitro-1,3,5-triazine (RDX). The parameters were material specific, but the reaction mechanism for all seven explosives were all the same. In the current work, we apply the same approach to seven explosives that contain HMX.

Thermophysical parameters for the explosives models [3] include specific heat (C_p), thermal conductivity (k) bulk density (ρ_b), theoretical maximum density (ρ_{co}), and the mass fraction of HMX. Kinetic parameters include the pressure exponent (n), steric factor (m), normalized activation energy (E), distribution parameter (σ), and rate acceleration caused by melting HMX (λ_m). The reaction enthalpy was determined using the product species hierarchy determined with TIGER [4] along with the species formation enthalpies (h_f).

Parameters needed for the pressure (P) calculation include the product molecular weights (M_w) as well as thermal strain ($\Delta\varepsilon_t$) determined with the volumetric expansion coefficient (β_v) and mechanical strain ($\Delta\varepsilon_m$) determined using the solid (ρ_s) and liquid densities (ρ_l) of RDX. Other mechanical parameters include the bulk modulus (K), Youngs modulus (E), and Poisson's ratio (ν) which were determined consistently using the longitudinal sound speed (S_L) and shear sound speeds (S_S).

The success of the one-step UCM/MMP for both the RDX [3] and HMX explosives (current work) is attributed to the flexible form of the distributed rate expression which can be

tuned to represent reaction forms ranging from diffusion-limited reactions that decelerate over time to auto-catalytic reactions which accelerate with the extent of reaction. The pressure-dependent term in the rate expression can also cause auto-catalytic behavior in confined systems. The purpose of this paper is to validate the simplified 1-step UCM/MMP model using seven explosives that contain HMX. Detailed derivation of the conductive energy equation and mechanics equation are beyond the scope of the present work, but the interested reader can find further information including derivations in [2] and [3].

The remainder of this paper will 1) present model parameters for the seven HMX-containing explosives, 2) parameterization of the kinetic model, 3) validation and 4) concluding discussion.

UCM/MMP model parameters

The UCM/MMP model is a solution of the conductive energy equation (Eq. 1) with source terms for explosive decomposition ($r_x h_r$) as well as melting ($\dot{q}_{melt}$). A method-of-lines code [5] with adaptive gridding is used to solve the equations.

$$\rho C_p \frac{\partial T}{\partial t} = \nabla \cdot (k \nabla T) + r_x h_r + \dot{q}_{\beta-\delta} + \dot{q}_{melt} \quad (1)$$

$$r_x = \frac{d[X]}{dt} = 1.586 \times 10^{15} \left(\frac{P}{P_o}\right)^n \lambda T^m \exp\left[-\frac{(E+\xi\sigma)}{T}\right] [X] \quad (2)$$

In Eq. (2), the inverse of the standard normal distribution (x) is used to make the reactions self-accelerating or autocatalytic. The positive sign following the normalized activation energy (E in Eq. 2) causes the activation energy to decrease with the extent of reaction resulting in rate acceleration (for a negative value of σ). Figure 1 shows the inverse of the standard normal distribution calculated with the Microsoft Excel function "x = NORM.INV(X/X$_o$,0,1)".

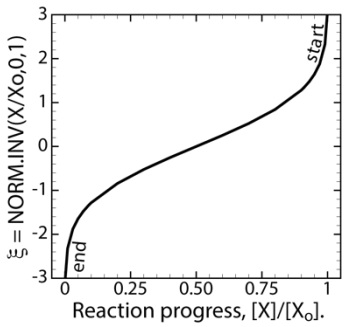

Fig. 1 ξ as a function of reaction.

Many of the parameters in Eq. (1) and Eq. (2) are given in Tables 1-5. The pressure-dependent distributed rate (r_x) in Eq. (2) is used to couple the energy equation to the displacement equation for a spherically symmetric linear elastic material surrounding a pressurized hollow sphere as shown in Fig. 1. Pressure (P) is the coupling variable and is determined using the density within the pressurizing defect.

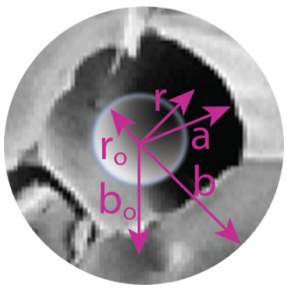

Fig. 2 Defect in explosive.

Table 1 *Some basic properties of explosives containing HMX*

Name	Comp. (wt.%), formula	Mw_x g/mol	O_2 bal.	ρ_{co}, kg/m^3	h_f kJ/mol	D^b km/s	T_a K
EDC-37	HMX/NC/K10 (91/1/8) $C_{4.46}H_{7.96}N_{7.3}O_{7.66}$	286.7	-29.2	1858	50.6	8.82	2845
HMX	HMX (100) $C_4H_8N_8O_8$	296.2	-21.6	1905	75.0	9.18	2920
LX-07	HMX/Viton-A® (90/10) $C_{4.48}H_{7.89}N_{7.36}O_{7.34}F_{1.05}$	302.2	-26.7	1899	-156.1	8.72	2827
LX-10	HMX/Viton-A® (95/5) $C_{4.25}H_{7.98}N_{7.68}O_{7.69}F_{0.52}$	299.6	-24.2	1902	-39.4	8.94	2882
LX-14	HMX/Estane® (95.5/4.5) $C_{4.4}H_{8.44}N_{7.48}O_{7.7}$	289.3	-29.5	1854	18.3	8.84	2809
PBX 9501	HMX/Estane®/NP (95/2.5/2.5) $C_{4.3}H_{8.34}N_{7.62}O_{7.87}$	292.7	-26.9	1859	27.2	8.75	2850
PBXN-9	HMX/PB/DOA (92/2/6) $C_{4.8}H_{9.32}N_{6.84}O_7$	274.8	-42.2	1755	11.1	8.18	2550

Table 2 *Reaction hierarchy for pre-ignition reactions*

Name	Equilibrium reactions, gas mol. wt. (Mw_G) heats of formation (h_f), and reaction enthalpies (h_r)
EDC-37	$C_{4.46}H_{7.96}N_{7.32}O_{7.66}$ (EDC-37) → 3.66 N_2 + 3.54 H_2O + 2.06 CO_2 + 0.22 CH_4 + 2.18 C EDC-37 → 9.48 G + 2.18 C Mw_G = 27.5 g/mol; $h_{f,G}$ = -177.5 kJ/mol; $h_{f,EDC37}$ = 50.6 kJ/mol; h_r = -1734 kJ/mol (exothermic)
HMX	$C_4H_8N_8O_8$ (HMX) → 4 N_2 + 3.6 H_2O + 2.2 CO_2 + 0.2 CH_4 + 1.6 C HMX → 10 G + 1.6 C Mw_G = 27.7 g/mol; $h_{f,G}$ = -175.1 kJ/mol; $h_{f,HMX}$ = 75 kJ/mol; h_r = -1826 kJ/mol (exothermic)
LX-07	$C_{4.48}H_{7.89}N_{7.36}O_{7.34}F_{1.05}$ (LX-07) → 3.68 N_2 + 3.10 H_2O + 2.12 CO_2 + 0.16 CH_4 + 1.05 HF + 2.2 C LX-07 → 10.11 G + 2.2 C Mw_G = 27.3 g/mol; $h_{f,G}$ = -186.1 kJ/mol; $h_{f,LX7}$ = -156.1 kJ/mol; h_r = -1726 kJ/mol (exothermic)
LX-10	$C_{4.25}H_{7.98}N_{7.68}O_{7.69}F_{0.52}$ (LX-10) → 3.84 N_2 + 3.35 H_2O + 2.17 CO_2 + 0.15 CH_4 + 0.52 HF + 1.89 C LX-10 → 10.07 G + 1.89 C Mw_G = 27.5 g/mol; $h_{f,G}$ = -180.7 kJ/mol; $h_{f,LX10}$ = -39.4 kJ/mol; h_r = -1780 kJ/mol (exothermic)
LX-14	$C_{4.4}H_{8.44}N_{7.48}O_{7.7}$ → 3.74 N_2 + 3.72 H_2O + 1.99 CO_2 + 0.25 CH_4 + 2.16 C LX-14 → 9.83 G + 2.16 C Mw_G = 27.3 g/mol; $h_{f,G}$ = -176.3 kJ/mol; $h_{f,LX14}$ = 26.9 kJ/mol; h_r = -1760 kJ/mol
PBX 9501	$C_{4.3}H_{8.34}N_{7.62}O_{7.87}$ (PBX 9501) → 3.81 N_2 + 3.73 H_2O + 2.07 CO_2 + 0.22 CH_4 + 2.01 C PBX 9501 → 9.83 G + 2.01 C Mw_G = 27.3 g/mol; $h_{f,G}$ = -176.3 kJ/mol; $h_{f,PBX9501}$ = 27.2 kJ/mol; h_{rxn} = -1760 kJ/mol (exothermic)
PBXN-9	$C_{4.8}H_{9.32}N_{6.84}O_7$ (PBXN-9) → 3.42 N_2 + 3.96 H_2O + 1.52 CO_2 + 0.35 CH_4 + 2.93 C PBXN-9 → 9.25 G + 2.93 C Mw_G = 25.9 g/mol; $h_{f,G}$ = -171.0 kJ/mol; $h_{f,PBXN9}$ = 11.09 kJ/mol; h_r = -1593 kJ/mol (exothermic)

Table 3 *Thermophysical properties* [6][a]

Name	T, K	C_p, J/kgK	k, W/mK (ρ_b, kg/m^3)		
EDC-37	300	990	0.31 (1834)		
	320	1082	0.37 (1834)		
	349	1216	0.37 (1834)		
HMX	300	1094	0.25 (1630)	0.15 (1150)	
	623	1760	0.25 (1630)	0.15 (1150)	
LX-07	300	1206	0.35 (1864)		
	441	1735	0.35 (1864)		
	447	1758	0.24 (1864)		
	700	2706	0.24 (1864)		
LX-10	300	1206	0.50 (1844)	0.17 (880)	
	441	1735	0.50 (1844)	0.17 (880)	
	447	1758	0.30 (1844)	0.15 (880)	
	700	2706	0.30 (1844)	0.15 (880)	
LX-14	300	1084	0.32 (1780)	0.26 (1550)	0.13 (854)
	441	1550	0.32 (1780)	0.26 (1550)	0.13 (854)
	447	1570	0.27 (1780)	0.19 (1550)	0.13 (854)
	700	2406	0.27 (1780)	0.19 (1550)	0.13 (854)
PBX 9501	300	1084	0.33 (1778)	0.23 (1582)	0.13 (856)
	441	1550	0.33 (1778)	0.23 (1582)	0.13 (856)
	447	1570	0.21 (1778)	0.21 (1582)	0.11 (856)
	700	2406	0.21 (1778)	0.21 (1582)	0.11 (856)
PBXN-9	300	1084	0.33 (1753)		
	441	1550	0.33 (1753)		
	447	1570	0.21 (1753)		
	700	2406	0.21 (1753)		

[a]Temperature dependent properties are interpolated linearly with constant extrapolation. The listed densities in parenthesis are the averages of several SITI runs.

Table 4 *Kinetic parameters*

Name	lnA[a]	n	m	E[b], K	σ, K	ω_{HMX}	HMX: λ_m
EDC-37	35	0.5	-2	15030	-1000	0.91	10
HMX	35	0.33	-2.5	14265	-500	1	10
LX-07	35	0.33[c]	0	21715	-750	0.90	2
LX-10	35	0.29[c]	0	21886	-500	0.95	2
LX-14	35	0.42	-2	14985	-700	0.955	2
PBX 9501	35	0.3	-2	15348	-700	0.95	20
PBXN-9	35	0.3[c]	-2	14838	-900	0.92	20

[a] "A" is the prefactor or frequency factor which is 1.586×10^{15} in Eq. (2).
[b]Normalized activation energy using the gas constant, R.
c Pressure exponent guessed due to either lack of vented data or inadvertent vent plugging.

Table 5 *Mechanics parameters*

Name	ρ_{co}, kg/m^3	S_L, m/s	S_S, m/s	K, GPa	E, GPa	ν	β, 1/K	ϕ_{HMX}	$\phi_{HMX}\Delta\tilde{\varepsilon}_{\beta-\delta}$[b]
EDC-37	1858	1.66	1.09	10.1	6.1	0.40	0.000131	0.89	0.059
HMX	1905	2.78	1.39	9.8	9.9	0.33	0.000131	1.00	0.067
LX-07	1899	2.80	1.39	10.0	9.8	0.34	0.000131	0.90	0.060
LX-10	1902	2.79	1.38	10.0	9.7	0.34	0.000131	0.95	0.064
LX-14	1854	2.89	1.47	10.1	10.7	0.32	0.000131	0.93	0.062
PBX 9501	1859	2.97	1.39	11.4	9.6	0.36	0.000131	0.93	0.062
PBXN-9	1755	3.08	1.66	10.2	12.5	0.30	0.000131	0.85	0.057

[b]The mechanical strain ($\Delta\tilde{\varepsilon}_{\beta-\delta} = 0.067$) is associated with the β–δ polymorphic transition between 441 and 447 K. This transition is made smoothly by using a cosine ramp function similar to that shown in Eq. (4).

The variables r_o, r, and "a" represent the initial defect radius, the defect radius accounting for decomposition but not mechanical displacement, and the radius accounting for both decomposition and mechanical displacement, respectively. The evolving defect gas density can be determined from the gas mass (indirectly from Eq. 2) and pore volume ($\frac{4}{3}\pi a^3$). The pore pressure is then determined from gas density (ρ) and a gas equation of state, e.g., $P = \rho RT/M_w$. The pore is assumed to fail when the pressure reaches 5 MPa whereafter the pore transitions from being closed to open. Pressure within the open pore is based on the total open pore gas volume and can include any headspace volume where pressure is typically measured.

The energy sink associated with the β–δ polymorphic phase change and HMX melting is accounted for by using an effective capacitance method. These phase changes occur over a temperature range with the lower temperature being the solidus temperature (T_S) and the upper temperature being the liquidus temperature (T_L). The latent energy is released smoothly between the T_S and T_L using a Gaussian distribution to account for both caloric and latent contributions to the transient heat conduction term in Eq. (1).

$$C_{eff} = C_p + \frac{\omega h_l}{\sigma\sqrt{2\pi}} e^{-\frac{z^2}{2}} \text{ with } \sigma = \frac{(T_m - T_S)}{3},\ T_m = \frac{(T_L + T_S)}{2}, \text{ and } z = \frac{(T - T_m)}{\sigma} \tag{3}$$

The effective capacitance method is used for the β–δ phase change in HMX as well as for melting HMX. In Eq. (3), ω represents the mass fraction of HMX. The variable h_l represents the latent enthalpy associated with either the β–δ phase change (h_l = 33000 J/kg) or melting (h_l = 236000 J/kg). The solidus and liquidus temperatures for the β–δ phase change is 441K and 447 K, and for melting is 529 K and 531 K, respectively.

Rate acceleration caused by phase change is usually significant when the boundary temperature exceeds the melting point of HMX. This acceleration is modeled using a rate multiplier, λ, which is 1 at T_S and λ_m at T_L. The multiplier, λ_m is given in Table 4. The following cosine ramp function was used to smoothly transition between these two temperatures for HMX:

$$\lambda = \begin{cases} 1, & T \le T_S \\ 1 + 0.5\left(1 - [\lambda_m - 1]\cos\left[\pi\frac{(T - T_S)}{(T_S - T_L)}\right]\right) & T_S < T < T_L \\ \lambda_m & T \ge T_L \end{cases} \tag{4}$$

Only the basic equations are given in Eq. (1) and Eq. (2), and the complete derivation and all auxiliary equations are beyond the scope to this proceeding. However, the interested reader can find all equations including derivation in references [2, 7]. Tables 1-5 provide the

parameters for UCM/MMP model for the 7 HMX-based explosives. These tables include basic properties of the explosives, reaction hierarchy, thermophysical properties, kinetic parameters, and mechanical properties.

Parameterization

We have simplified the UCM from reference [1] by reducing the reaction set from four to one without a loss of accuracy. In some cases, the simpler UCM model fits the available cookoff data better. We attribute the better fit to capturing the interaction between decomposition products that originate from both the binder material and the HMX. Another reason for the better fit is ease of fitting a single rate compared to fitting four rate expressions.

Most of the parameters listed in Tables 1-6 are obtained from either the literature or from fitting cookoff data. Usually, the intrinsic properties of the explosive such as composition and molecular weight are known. The reaction hierarchy is determined using equilibrium calculations at 400 K and 0.1 MPa. We have found that the product hierarchy is similar even at temperatures and pressures spanning both slow and fast cookoff conditions. Physical properties for the current work were obtained primarily from the literature [6]. The bulk modulus, elastic modulus, and Poisson's ratio were obtained from the longitudinal and shear sound velocities which were obtained from various references [8, 9, 10]. Sound speeds for PBXN-9, LX-07, LX-10, and LX-14 were estimated using a linear fit of sound speed data from other explosives in Marsh's handbook [8], e.g., given ρ_{co} in g/cm^3 the sound speed in km/s was estimated as $S_L = -1.92\rho_{co} + 6.44$ and $S_S = -1.86\rho_{co} + 6$. The volumetric expansion coefficient and mechanical strain associated with the β-δ transition ($\Delta\tilde{\varepsilon}_{\beta-\delta}$) were taken from [11].

Cookoff data used for parameter estimation and validation were obtained from the Sandia Instrumented Thermal Ignition (SITI) and One-Dimensional-Time to eXplosion (ODTX) experiments shown schematically in Fig. 3. The SITI experiment confines two 2.54 cm diameter by 1.27 cm high cylinder of explosive. Nine type K 127 μm diameter thermocouples with measuring point located at radial positions in mm of 0, 1.70, 2.55, 3.40, 4.25, 5.11, 5.96, 8.81, and 11.7 are placed between the two explosive cylinders. The outer surface of the SITI apparatus is 7.62 cm diameter by 4.58 cm tall and is heated using rope heaters controlled by a thermocouple on the lateral surface. The external aluminum surface is heated to a set point temperature, T_{sp}, in 600 s and held until the explosive thermally ignites. Two expansion gaps that are above and below the explosive are also machined into the

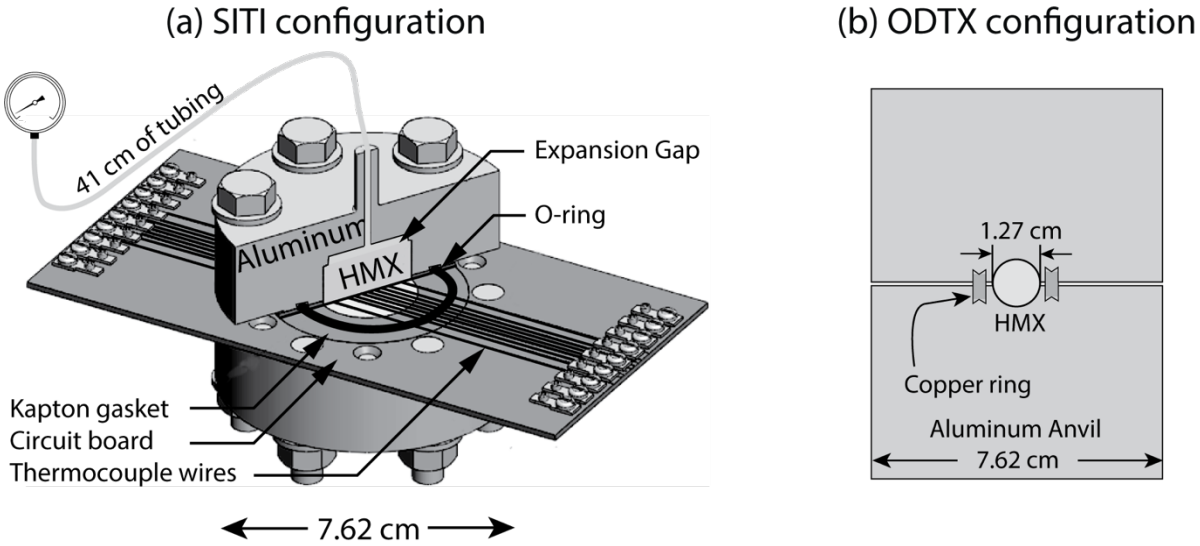

Fig. 3 (a) SITI and (b) ODTX configurations.

confining aluminum. Each expansion gap has a diameter of 2.22 cm and is nominally 0.16 cm tall. In some experiments the gap was larger, up to 0.55 cm. For sealed experiments the gap volume as well as the pressure tubing volume (~0.09 cm^3) affects the ignition time.

The ODTX experiment confines a 1.27 cm diameter sphere with constant temperature anvils as shown in Fig. 3(b). Expansion volumes are not reported for the ODTX experiments, but we estimate the excess gas volume at about 0.1 cm^3 based on thermal expansion of the confining aluminum anvils and gaps between the explosive and copper gasket. Two preheated 7.62 cm diameter by 5.08 cm high aluminum cylinders hydraulically confine a spherical sample to 150 MPa in a machined cavity with a knife edge channel surrounding the explosive. A copper gasket is used to retain the decomposition gases within the cavity. At time zero, preheated anvils are quickly placed around the explosive providing a constant temperature boundary temperature.

Thermal ignition data is not required for most of the parameters in Tables 1-6 except for the kinetic parameters n, m, E, σ, and λ_m. For simplification, the preexponential coefficient (A) in Eq. (2) is not varied but kept constant at $\ln A = 35$ or $A = 1.586\times10^{15}$ s^{-1}, which we have found works well for a number of energetic materials. Setting a constant preexponential also prevents problems associated with kinetic compensation where changes in A can be compensated for by changes in E. Both vented and sealed SITI data from low-density explosives where decomposition gases can flow throughout the bed are best for determining n since the temporal behavior of the headspace pressure can be measured. For higher density explosives the gases are sometime retained within the explosive and the temporal behavior of the measured pressure is not as useful.

Several iteration procedures are used to obtain the kinetic coefficients: 1) vented and sealed low-density SITI runs are used to determine *n*, *E*, and σ, 2) multiple vented and sealed SITI data are used to determine *m* which influences the slope of the SITI ignition plot of 1000/T vs. log t_{ign}, and 3) ODTX data is used to determine slope changes at the melting point to set λ_m. The iteration procedure begins by choosing σ and setting *n* to zero, and then determining the normalized activation energy *E* that matches ignition time for a vented SITI experiment. The pressure exponent, *n*, is then determined from a sealed SITI experiment. If the pressure profile does not match, then σ can be reset and adjusted until the shape of the measured pressure profile is predicted adequately. After the initial iteration procedure, the overall ignition plot (1000/T vs log t_{ign}) can be used to set λ_m which usually does not affect the SITI results.

Validation

The model was used to predict both internal temperature and pressure profiles as well as thermal ignition time for the seven HMX-based explosives as shown in Figs. 4 and 5. The plots on the left-hand side of these figures show predicted and measured pressure at nine radial locations for a single SITI run for each explosive. Temperature is well behaved and shows expected plateaus as the HMX changes from the β polymorph to the δ polymorph. Internal pressure increases until the pore failure pressure (5 MPa) is reached. Then, the pressure decreases as the gases mix with the open pore explosive and headspace volumes. The pressure within the damaged explosive and headspace volume usually matches the measured pressure. Figures 2 and 3 also show good agreement between predicted and measured thermal ignition times for both the SITI experiments (middle plots) and the ODTX experiments (right-hand plots).

There are some caveats associated with some of the older SITI data. For example, there are only two sealed SITI runs for EDC-37 and no vented data. Similarly, there were no vented SITI runs for LX-07. In addition, the vented runs for PBXN-9 plugged and viable vented date were not obtained. The pressure exponent n for EDC-37, LX-07, and PBXN-9 were assumed to be similar to the other explosives containing HMX. There was also an excursion observed in the EDC-37 SITI data that was likely caused by exothermic decomposition of the NC which seems to be small and not an issue for EDC-37. However, a similar excursion was observed in the PBX 9501 data which might be problematic for systems that are tightly sealed as discussed further in [11]. We recommend caution when using the EDC-37, LX-07, and PBXN-9 models without further vented data to for better pressure exponent estimates.

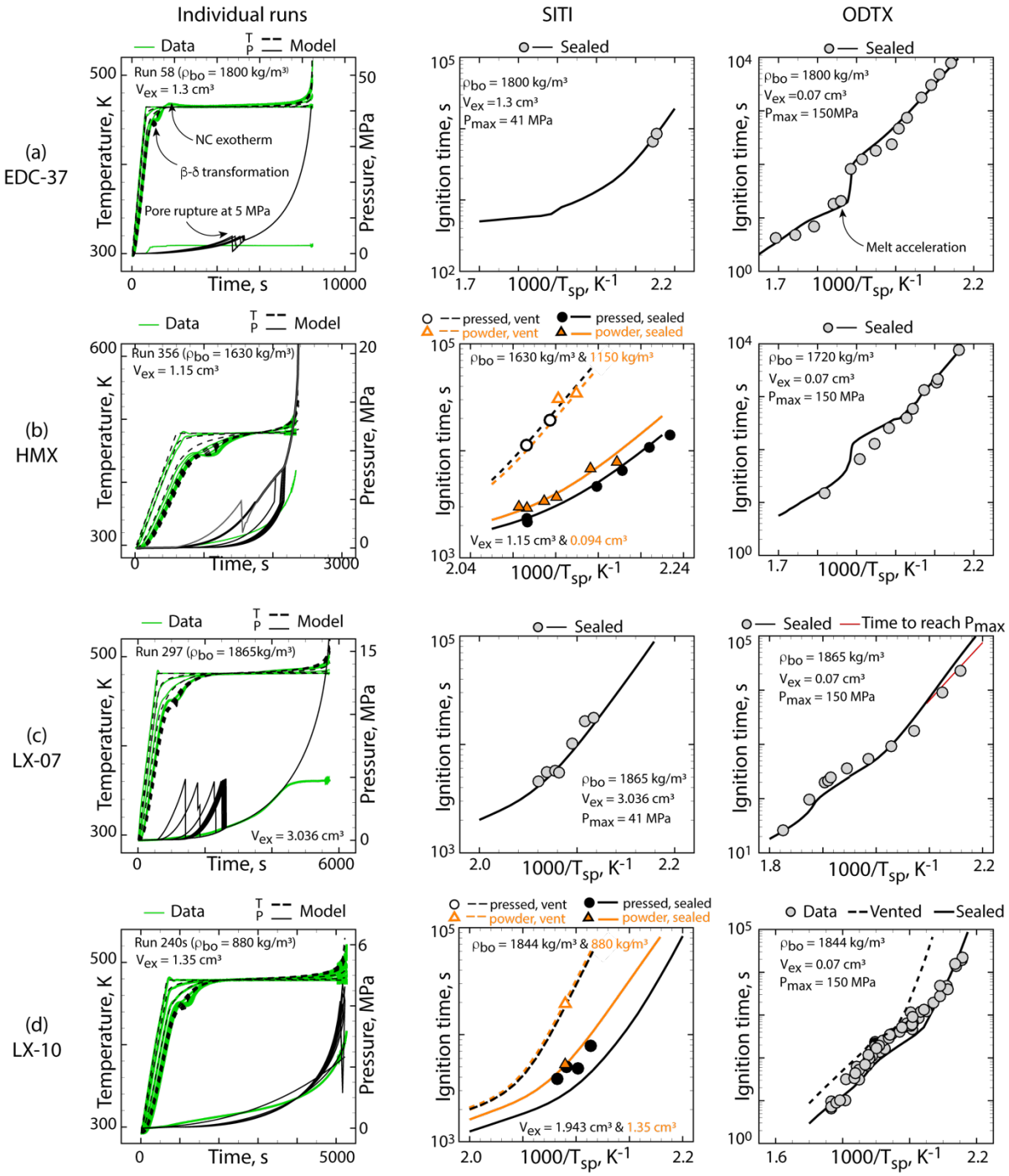

Fig. 4 Individual runs showing predicted and measured pressure, thermal ignition time for the SITI experiments, and thermal ignition times for the ODTX experiments for (a) EDC-37, (b) Comp-C4, (c) PBX 9407, and (d) LX-10. More detail regarding the SITI data can be found in [12, 13]. Details regarding the ODTX data can be found in [14, 15].

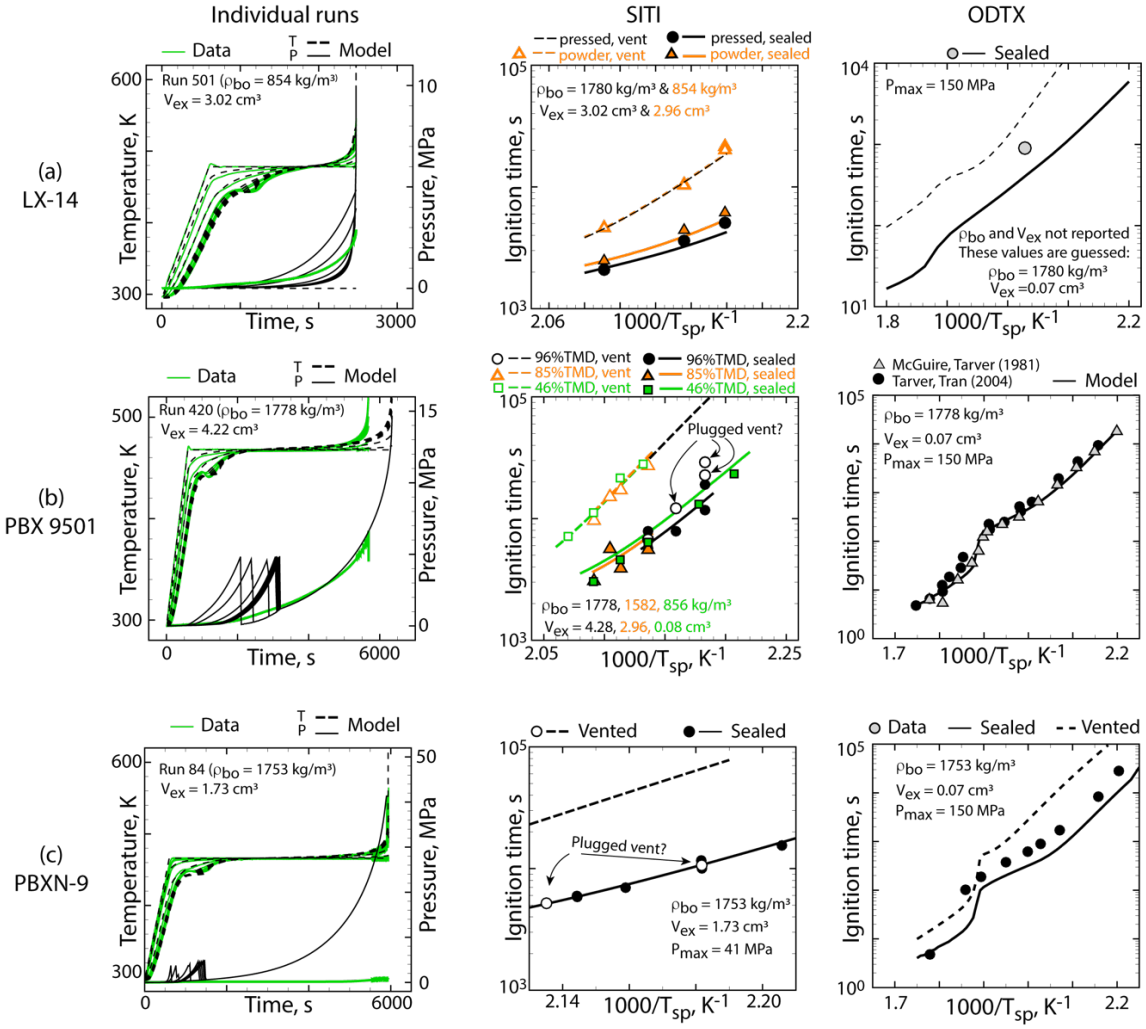

Fig. 5 Individual runs showing predicted and measured pressure, thermal ignition time for the SITI experiments, and thermal ignition times for the ODTX experiments for (a) LX-14, (b) PBX 9501, and (c) PBXN-9. More detail regarding the SITI data can be found in [16, 11]. Details regarding the ODTX data can be found in [14, 15, 17].

Summary and conclusions

The UCM/MMP model has been simplified and used to model thermal ignition of seven explosive containing HMX: EDC-37, HMX (pure), LX-07, LX-10, LX-14, PBX 9501, and PBXN-9. The reaction model uses a single first-order decomposition mechanism utilizing a pressure dependent distributed reaction rate based on the reaction extent. Pressure was determined using a micromechanics pressurization model. These results complement work presented at the 2nd International Explosive Conference [3] where we used the same model form for seven explosives containing RDX. These 14 explosive models that accurately replicate experimental data from multiple laboratories support the hypothesis that a one-step pressure-dependent reaction model is sufficient to replicate thermal ignition in a wide variety of explosives.

Acknowledgements

We would also like to thank Shane Snedigar and Michael Oliver for running the SITI experiments, Farhan Rahman and John Tencer for internal review, and Jeremy Lechman for management support.

References

[1] M. L. Hobbs, M. J. Kaneshige and W. W. Erikson, "A Universal Cookoff Model for Explosives," in *50th International Annual Conference of the Fraunhofer ICT*, Karlsruhe, 2019.

[2] M. L. Hobbs, J. A. Brown, M. J. Kaneshige and C. Aviles-Ramos, "A Micromechanics Pressurization Model for Cookoff," *Propellants Explos. Pyrotech.,* vol. 47, no. 2, pp. 1-15, 2022.

[3] M. L. Hobbs, M. J. Kaneshige and W. W. Erikson, "UCM/MMP cookoff models for explosives containing RDX," in *Fundamental Science of Explosives and Other Energetic Materials: 2nd Internatoinal Explosives Conference*, London, The Royal Society of Chemistry, 2024, pp. 1-14.

[4] M. L. Hobbs, R. G. Schmitt, H. K. Moffat and Z. Lawless, "JCZS3--an improved database for EOS calculations," in *16th International Detonation Symposium*, Cambridge, 2018.

[5] R. J. Gross, M. R. Baer and M. L. Hobbs, "XCHEM-1D A heat transfer/chemical kinetics computer program for multilayered reactive materials," Sandia National Laboratories, SAND93-1603, UC-741, Albuquerque, 1993.

[6] Z. Lawless, M. L. Hobbs and M. J. Kaneshige, "Thermal Conductivity of Energetic Materials," *Journal of Energetic Materials,* vol. 38, no. 2, pp. 214-239, 2020.

[7] M. L. Hobbs, J. A. Brown, M. J. Kaneshige and C. Aviles-Ramos, "Cookoff of powdered and pressed explosives using a micromechanics pressurization model," *Propell. Explos. Pyrot.,* vol. 47, pp. 1-16, 2022.

[8] S. P. Marsh, LASL Shock Hugoniot Data, Berkeley: University of California Press, 1980.

[9] J. J. Dick, A. R. Martinez and R. S. Hixson, "Plane impact response of PBX 9501 and its components below 2 GPa," Los Alamos National Laboratory Report LA-13426-MS UC-741, Los Alamos, 1998.

[10] J. J. Haycraft, L. L. Stevens and C. J. Eckhardt, "The elastic constants and related properties of the energetic material cyclotrimethylene trinitramine (RDX) determined by Brillouin scattering," *J. Chem. Phys.,* vol. 124, p. 024712, 2006.

[11] M. L. Hobbs, M. J. Kaneshige and W. W. Erikson, "Modeling the measured effect of a nitroplasticizer (BDNPA/F) on cookoff of a plastic bonded explosive (PBX 9501)," *Combust. Flame,* vol. 173, pp. 132-150, 2016.

[12] M. L. Hobbs, J. Baker, M. D. Cook, M. J. Kaneshige, S. C. Schumacher and C. Stennett, "Cookof Reaction Violence," in *Future Developments in Explosives and Energetics: 1st International Explosives Conference*, London, The Royal Society of Chemistry, 2023, pp. ISBN-13 9781788017855.

[13] C. Aviles-Ramos, "Parameterization of a Cookoff Model for LX-07," in *Sixteenthe International Detonation Symposium*, Cambridge, 2018.

[14] R. R. McGuire and C. M. Tarver, "Chemical decomposition models for the thermal explosion of confined HMX, TATB, RDX, and TNT explosives," in *7th International Symposium on Detonation*, Annapolis, 1981.

[15] C. M. Tarver and T. D. Tran, "Thermal decomposition models for HMX-based plastic bonded explosives," *Combust. Flame,* vol. 137, pp. 50-62, 2004.

[16] M. L. Hobbs, M. J. Kaneshige, W. W. Erikson and K. T. Meirs, "Gas retention in an HMX-based explosive (LX-14)," *Sci. Tech. Energetic Materials,* vol. 79, no. 2, pp. 35-42, 2018.

[17] E. A. Glasco, J. L. Maienschein, A. K. Burnham, J. G. Boerner, P. C. Hsu and A. P. Wemhoff, "PBXN-9 Ignition Kinetics and Deflagration Rates," in *55th JANNAF Propulsion Meeting*, Newton, 2008.